Table 1 Comparison of theoretical models and experiment at $\alpha = 14.85$ deg

$h = 0.7$, $X_B = 0.5$	min C_P	C_L	$h = 1$, $X_B = 0.5$	min C_P	C_L
Doublet	−8.43	1.955	Doublet	−8.75	1.953
Source/sink	−7.00	1.876	Three-vortex	−10.6	1.997
Eq. (2)	−∞	1.610	Eq. (2)	−∞	1.610
Eq. (3)	0	0.324	Eq. (3)	0	0.324
Experiment[7]	−0.69	0.883	Experiment[7]	−0.69	0.883

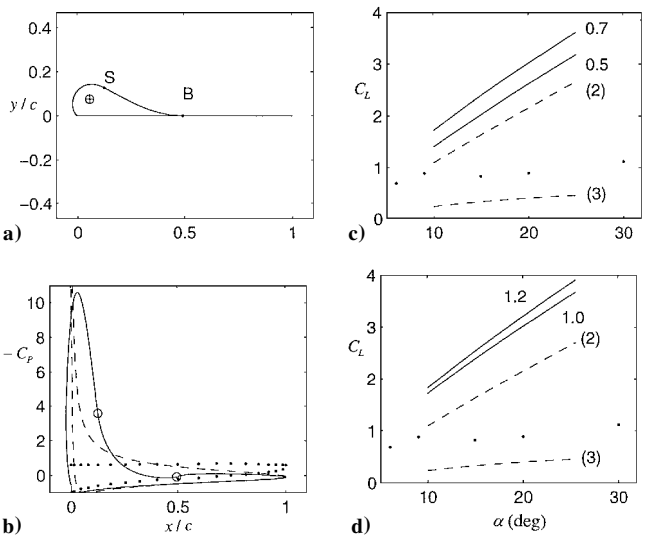

Fig. 4 Three-vortex model at $\alpha = 14.85$ deg (●, experiment[7]): a) Z plane, ⊕, vortex; b) ——, present; – – –, Eq. (1), $h = 1$, $X_B = 0.5$; c) C_L vs α for $h = 1$: $X_B = 0.7, 0.5$; and d) C_L vs α for $X_B = 0.7$: Eq. (1) $h = 1.2, 1.0$.

edge the present model offers $C_P = 0.098$, which is higher than those values from Eq. (1) and the experiment.[7] The lift coefficient is increased by 16.5%. At given values of X_B and h, C_L increases with α, as shown in Figs. 3c and 3d.

The location of the external vortex, shape of bounding streamline, fence and plate for the three-vortex model are shown in Fig. 4a at $\alpha = 14.85$ deg, $h = 1$, and $X_B = 0.5$. The bubble has $y_{\max}/c = 0.144$ at $x/c = 0.067$ and trailing edge of $C_P = 0.117$, both slightly larger than $y_{\max}/c = 0.1311$ at $x/c = 0.092$ and $C_P = 0.102$ from the doublet model under the same condition. The finite suction peak at the leading edge and finite pressure gradients at S and B are shown in Fig. 4b. In comparison with the attached flow model, C_L is increased by 24.1%. At fixed values of X_B and h, variations of C_L with α are depicted in Figs. 4c and 4d, respectively. Table 1 compares some results from the theoretical models and experimental measurements.

Conclusion

An analytical method is proposed for augmenting the lift on a flat plate experiencing massive separation on its suction side. At any positive angle of attack, the separated flow at the leading edge is made to reattach smoothly to a forward-facing fence by suitable mathematical singularities subject to available boundary conditions. A bounding streamline, which emanates from the separation point and terminates at the tip of the fence joining the plate tangentially on its upper surface to prevent any unnecessary stagnated flow, increases the camber and thickness of the plate. Finite velocity is enforced at each of the critical points of the conformal mapping, namely the tip of the fence and leading and trailing edges of the plate. In addition, the condition of finite pressure gradient at reattachment is satisfied where applicable. Numerical results from varying the length of the fence and its location with respect to the leading edge suggest that lift on the flat plate is enhanced, when compared with the predictions from the attached flow model by Kutta–Joukowsky, the separated flow theory by Kirchhoff–Helmholtz, and measurements by Fage and Johansen.

References

[1]Korbacher, G. K., "Aerodynamics of Powered High-Lift Systems," *Annual Review of Fluid Mechanics*, Vol. 6, 1974, pp. 319–358.

[2]Huang, M., and Chow, C., "Trapping of a Free Vortex by Joukowski Airfoils," *AIAA Journal*, Vol. 20, No. 3, 1982, pp. 292–298.

[3]Rossow, V. J., "Aerodynamics of Airfoils with Vortex Trapped by Two Spanwise Fences," *Journal of Aircraft*, Vol. 31, No. 1, 1994, pp. 146–153.

[4]Finaish, F., and Witherspoon, S., "Aerodynamic Performance of an Airfoil with Step-Induced Vortex for Lift Augmentation," *Journal of Aerospace Engineering*, Vol. 11, Jan. 1998, pp. 9–16.

[5]Traub, L. W., "Efficient Lift Enhancement of a Blunt Edged Delta Wing," *The Aeronautical Journal*, Nov. 1997, pp. 439–445.

[6]Werle, H., "Le Tunnel Hydrodynamique au Service de la Recherche Aerospatiale," Publication No. 156, ONERA, France, 1974, (Photograph 35 in Van Dyke, M., *An Album of Fluid Motion*, The Parabolic Press, CA, 1988).

[7]Fage, A., and Johansen, F. C., "On the Flow of Air Behind an Inclined Flat Plate of Infinite Span," *Proceedings of the Royal Society of London*, A Vol. 116, Sept. 1927, pp. 170–197.

[8]Japan Society of Mechanical Engineers, *Visualized Flow*, Pergamon, Oxford, 1988 (Photograph 130), p. 79.

[9]Hurley, D. G., "The Use of Boundary Layer Control to Establish Free Streamline Flows," *Advances in Aeronautical Science*, Vol. 2, 1959, pp. 662–708.

[10]Yeung, W. W. H., and Parkinson, G. V., "A Theoretical Investigation of Enhanced Lift in the Presence of Thin Aerofoil Stall," *The Aeronautical Journal*, May 1999, pp. 237–244.

[11]Ormsbee, A. I., and Maughmer, M. D., "A Class of Airfoils Having Finite Trailing-Edge Pressure Gradients," *Journal of Aircraft*, Vol. 23, No. 2, 1986, pp. 97–103.

[12]Yeung, W. W. H., and Parkinson, G. V., "A Wake Singularity Potential Flow Model for Airfoils Experiencing Trailing-Edge Stall," *Journal of Fluid Mechanics*, Vol. 251, June 1993, pp. 203–218.

Moving-Wall Effect on Unsteady Boundary Layers

H. Dumitrescu* and V. Cardoş†
Caius Iacob Institute of Applied Mathematics, RO 70700, Bucharest, Romania

I. Introduction

MOVING-WALL effect for airfoils refers to the unsteady wall boundary condition, which may lead to different courses of leading-edge separation. An airfoil oscillating at large angles of attack presents a well-known case of dynamic stall, characterized by a delay in the onset of boundary-layer separation. Two contributions are responsible for this overall delay: one is caused by the beneficial accelerated flow effects on the developing boundary layer during the angle of attack increasing phase, and the other is caused by the moving-wall effect illustrated in Fig. 1 (Ref. 1).

As the leading edge moves upward during the upstroke, the boundary layer is strengthened and stall delayed because of the large difference in tangential wall velocities at the flow stagnation and separation points on the upper side of the airfoil. There the boundary layer has a fuller velocity profile and is, therefore, more difficult to separate. Figure 1 clearly shows that the moving-wall effect will be different for an airfoil oscillating in a uniform stream in pitching and plunging modes. Thus, when the effective angle of attack is increasing, the moving-wall effect is favorable for the pitching airfoil, whereas it is adverse for the equivalent plunging airfoil, with the nose in downward stroke. In spite of this fact and the experimental findings,[2] most dynamic stall analysis methods[3]

Received 23 June 1999; revision received 2 July 1999; accepted for publication 21 September 1999.

*Professor and Senior Researcher, Romanian Academy, P.O. Box 1-24.
†Senior Researcher, Romanian Academy, P.O. Box 1-24.

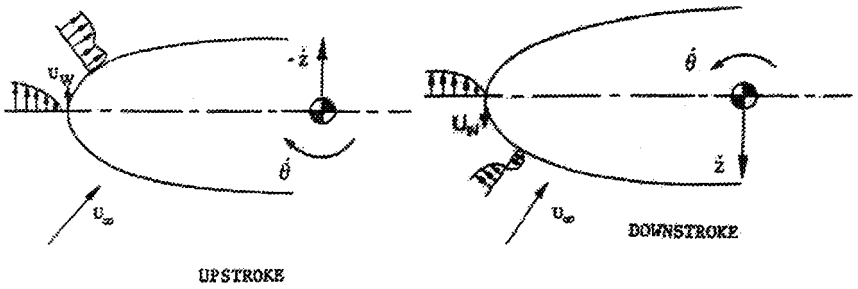

Fig. 1 Opposite moving-wall effect.

assume the similarity of these two motions expressed by Carta's equivalence relationship for the effective angle of attack.[4]

The differences between these two motions can be explained by the opposite moving-wall effects upon the boundary-layer separation. Therefore, the problem must be analyzed from the viewpoint of a body-fixed reference frame. The continuity equation and the dynamic equations of motion, for a fluid in motion relative to observer coordinates moving arbitrarily, will be displayed and discussed briefly for constant density and constant viscosity Newtonian fluids. It will be shown that the expression of the boundary-layer equations in this frame preserves essentially the same forms as in the common inertial case.

II. Boundary-Layer Equations

The continuity equation in the moving system is no different than in inertial coordinates

$$\nabla \cdot \boldsymbol{v} = 0 \tag{1}$$

On the other hand, the dynamic equations of motion contain four additional inertial terms—the Coriolis, centrifugal, linear, and angular acceleration terms—as follows:

$$K\frac{\partial \boldsymbol{v}}{\partial t} + (\boldsymbol{v}\cdot\nabla)\boldsymbol{v} = -\nabla p + \boldsymbol{F} + \frac{1}{Re}\nabla^2\boldsymbol{v} \tag{2}$$

where $\boldsymbol{F}$ denotes the sum of all apparent body forces resulting from linear $(\mathrm{d}^2\boldsymbol{R}/\mathrm{d}t^2)$ and angular $(\mathrm{d}\boldsymbol{\Omega}/\mathrm{d}t)$ accelerations of the noninertial reference frame

$$\boldsymbol{F} = -K\left[K\frac{\mathrm{d}^2\boldsymbol{R}}{\mathrm{d}t^2} + K\frac{\mathrm{d}\boldsymbol{\Omega}}{\mathrm{d}t}\times\boldsymbol{r} + 2\boldsymbol{\Omega}\times\boldsymbol{v} + K\boldsymbol{\Omega}\times(\boldsymbol{\Omega}\times\boldsymbol{r})\right]$$

Each term in Eqs. (1) and (2) has been appropriately nondimensionalized in terms of the relevant length scale L, the frequency of the oscillating motion ω, and a typical velocity scale U_∞. The two dimensionless parameters appearing in the equations are the reduced frequency $K = \omega L/U_\infty$ and the Reynolds number $Re = U_\infty L/\nu$. Further, the boundary-layer equations are obtained by using Prandtl's classic boundary-layer approximation.[5] Let x and z be the coordinates along the body wall and y normal to the wall. The thin-layer approximation $(v \ll u,\ \partial/\partial x,\ \partial/\partial z \ll \partial/\partial y)$ can be applied just as for the inertial case. Under these approximations the transverse velocity component v and the pressure variation across the layer $\partial p/\partial y$ are of order shear-layer thickness δ, provided the order of all inertial acceleration terms is no greater than unity. The net result is that the full equations of motion (1) and (2) are reduced to

$$\frac{\partial u}{\partial x} + \frac{\partial v}{\partial y} + \frac{\partial w}{\partial z} = 0 \tag{3}$$

$$K\frac{\partial u}{\partial t} + u\frac{\partial u}{\partial x} + v\frac{\partial u}{\partial y} + w\frac{\partial u}{\partial z} = -\frac{\partial p}{\partial x} + X_b + \frac{1}{Re}\frac{\partial^2 u}{\partial y^2}$$

$$K\frac{\partial w}{\partial t} + u\frac{\partial w}{\partial x} + v\frac{\partial w}{\partial y} + w\frac{\partial w}{\partial z} = -\frac{\partial p}{\partial z} + Z_b + \frac{1}{Re}\frac{\partial^2 w}{\partial y^2} \tag{4}$$

where (u, v, w) denote components of the velocity vector $\boldsymbol{v}$ along the coordinates (x, y, z), respectively, and (X_b, Z_b) are the tangential components of the apparent force $\boldsymbol{F}_b$, which in the boundary-layer flow equation has the approximate form

$$\boldsymbol{F}_b = -K\left[K\frac{\mathrm{d}^2\boldsymbol{R}}{\mathrm{d}t^2} + K\frac{\mathrm{d}\boldsymbol{\Omega}}{\mathrm{d}t}\times\boldsymbol{r}_b + 2\boldsymbol{\Omega}\times\boldsymbol{v} + K\boldsymbol{\Omega}\times(\boldsymbol{\Omega}\times\boldsymbol{r}_b)\right]$$

where $\boldsymbol{r}_b$ is the position vector on the body surface.

Because the pressure vanes are only along the boundary layer, not through it, the pressure gradient terms in Eqs. (4) are assumed to be known in advance from the outer inviscid flow

$$-\frac{\partial p}{\partial x} = K\frac{\partial U}{\partial t} + U\frac{\partial U}{\partial x} + W\frac{\partial U}{\partial z} - X_i$$

$$-\frac{\partial p}{\partial z} = K\frac{\partial W}{\partial t} + U\frac{\partial W}{\partial x} + W\frac{\partial W}{\partial z} - Z_i \tag{5}$$

Here (U, W) are components of the local freestream velocity $\boldsymbol{V}$ tangent to the body surface, and (X_i, Z_i) are tangential components of the apparent body force $\boldsymbol{F}_i$, which at the body surface, into the outer inviscid flow, is writtten

$$\boldsymbol{F}_i = -K\left[K\frac{\mathrm{d}^2\boldsymbol{R}}{\mathrm{d}t^2} + K\frac{\mathrm{d}\boldsymbol{\Omega}}{\mathrm{d}t}\times\boldsymbol{r}_b + 2\boldsymbol{\Omega}\times\boldsymbol{V} + K\boldsymbol{\Omega}\times(\boldsymbol{\Omega}\times\boldsymbol{r}_b)\right]$$

Replacing the pressure gradient expressions, Eqs. (5) into Eqs. (4), gives for the final forms of the x- and z-momentum equations

$$K\frac{\partial u}{\partial t} + u\frac{\partial u}{\partial x} + v\frac{\partial u}{\partial y} + w\frac{\partial u}{\partial z} = K\frac{\partial U}{\partial t} + U\frac{\partial U}{\partial x} + W\frac{\partial U}{\partial z} + X' + \frac{1}{Re}\frac{\partial^2 u}{\partial y^2}$$

$$K\frac{\partial w}{\partial t} + u\frac{\partial w}{\partial x} + v\frac{\partial w}{\partial y} + w\frac{\partial w}{\partial z} = K\frac{\partial W}{\partial t} + U\frac{\partial W}{\partial x} + W\frac{\partial W}{\partial z} + Z' + \frac{1}{Re}\frac{\partial^2 w}{\partial y^2} \tag{6}$$

where (X', Z') are tangential components of the force defect $\boldsymbol{F}'$ given by

$$\boldsymbol{F}' = \boldsymbol{F}_b - \boldsymbol{F}_i = 2K\boldsymbol{\Omega}\times(\boldsymbol{V} - \boldsymbol{v}) \tag{7}$$

Equations (3) and (6) are the noninertial equivalent to the inertial form for three-dimensional boundary-layer flows. The only additional term, Eq. (7), which represents the Coriolis effect induced by the rigid-body rotation, is important for atmospheric and oceanographic flows $(K \gg 1)$ under the influence of the rotation of the Earth. For two-dimensional plane motion the rotation vector is perpendicular to the plane, and the streamwise component of the Coriolis force $X' = 2K\Omega v$ can be neglected according to the

boundary-layerapproximation. Thus, the boundary-layerequations reduce to

$$\frac{\partial u}{\partial x} + \frac{\partial v}{\partial y} = 0 \tag{8}$$

$$K\frac{\partial u}{\partial t} + u\frac{\partial u}{\partial x} + v\frac{\partial u}{\partial y} = K\frac{\partial U}{\partial t} + U\frac{\partial U}{\partial x} + \frac{1}{Re}\frac{\partial^2 u}{\partial y^2} \tag{9}$$

The boundary-layer formulation in moving coordinates is the same as in the inertial case provided the forcing terms are evaluated at the edge of the boundary layer from the relative inviscid flow. Evolution of the boundary layer is then determined solely by history of the prescribed effective pressure gradient defined as

$$-\frac{\partial p^*}{\partial x} \equiv K\frac{\partial U}{\partial t} + U\frac{\partial U}{\partial x} = -\frac{\partial p}{\partial x} + X_i \tag{10}$$

The primary advantage of using this form is to reveal the combined effect of pressure and apparent body force on the developing boundary layer.

III. Potential Flow Equations

To estimate the viscosity effect, it is necessary to be able to calculate the unsteady boundary layer. This, in its turn, can only be performed if the pressure distribution along the moving body is available. Therefore, we are dealing with the calculation of the potential pressure distribution for an arbitrarily moving body in incompressible flow.

Consider a right cylinder as shown in Fig. 2. The coordinates $x_c y_c$ are locked on the cylinder, which generally is undergoing a combined forward motion with uniform velocity and incidence $\alpha[U_\infty e^{i(\alpha+\pi)}]$, horizontal oscillation $(U_h e^{i\alpha})$, vertical plunging oscillation $[U_v e^{i(\pi/2+\alpha)}]$, and pitching oscillation with angular velocity Ω. By transforming the cylinder (actually a thin airfoil) into a circle, the complex potential may be written using the boundary stream function Ψ. Letting the complex velocity $Q = U - iV$, the boundary function is given by

$$2i\Psi = \left[U_\infty Z e^{-i(\pi+\alpha)} - U_\infty \bar{Z} e^{i(\pi+\alpha)}\right] + \left(U_h Z e^{-i\alpha} - U_h \bar{Z} e^{i\alpha}\right) + \left[U_v Z e^{-i(\pi/2+\alpha)} - U_v \bar{Z} e^{i(\pi/2+\alpha)}\right] - i\Omega Z\bar{Z} \tag{11}$$

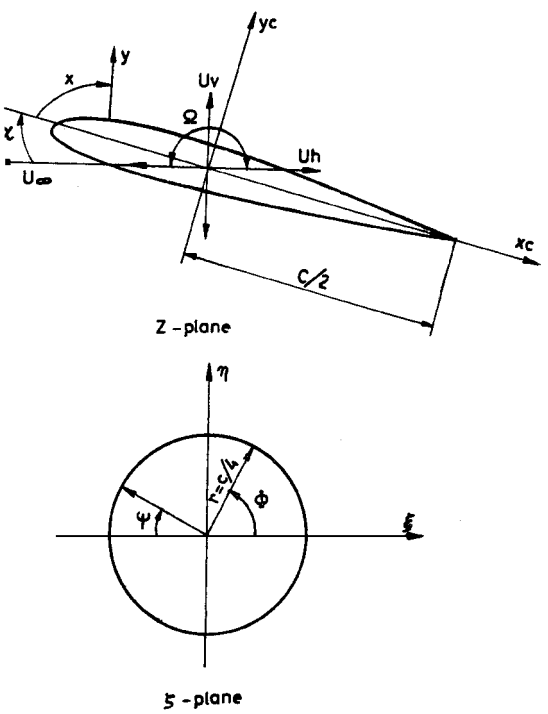

Fig. 2 Configuration of body motions.

Transforming to the circle plane $Z = f(\zeta)$, we obtain

$$2i\Psi = B(\varsigma) = \left[U_\infty e^{-i(\pi+\alpha)} f(\varsigma) - U_\infty e^{i(\pi+\alpha)} f(\varsigma)\right] + \left[U_h e^{-i\alpha} f(\varsigma) - U_h e^{i\alpha} f(\varsigma)\right] + \left[U_v e^{-i(\pi/2+\alpha)} f(\varsigma) - U_v e^{i(\pi/2+\alpha)} f(\varsigma)\right] - i\Omega f(\varsigma) f(\varsigma) \tag{12}$$

With the transformation $Z = \varsigma + r^2/\varsigma$, where $r = c/4$, the thin airfoil of chord c is transformed into a circle of radius $c/4$. Using the preceding transform and noting on the circle $\varsigma\bar{\varsigma} = r^2$, the boundary function becomes

$$B(\varsigma) = \left[U_\infty e^{-i(\pi+\alpha)} - U_\infty e^{i(\pi+\alpha)}\right][\varsigma + (r^2/\varsigma)] + \left[U_h e^{-i\alpha} - U_h e^{i\alpha}\right][\varsigma + (r^2/\varsigma)] + \left[U_v e^{-i(\pi/2+\alpha)} - U_v e^{i(\pi/2+\alpha)}\right][\varsigma + (r^2/\varsigma)] - i\Omega[\varsigma + (r^2/\varsigma)]^2 \tag{13}$$

which indeed is a function of ς alone.

Now the boundary function $B_1(\varsigma)$ contains only the negative powers of ζ and is equal to the complex potential. Thus,

$$B_1(\varsigma) = W(\varsigma) = -U_\infty\left[e^{-i(\alpha-\theta)} - e^{i(\alpha-\theta)}\right](r^2/\varsigma) + U_h\left[e^{-i(\alpha-\theta)} - e^{i(\alpha-\theta)}\right](r^2/\varsigma) - iU_v\left[e^{-i(\alpha-\theta)} - e^{i(\alpha-\theta)}\right](r^2/\varsigma) - i\Omega(r^4/\varsigma^2) \tag{14}$$

If there is circulation, we may add a vortex at the origin giving

$$B_1(\varsigma) = W(\varsigma) = -U_\infty\left[e^{-i(\alpha-\theta)} - e^{i(\alpha-\theta)}\right](r^2/\varsigma) + U_h\left[e^{-i(\alpha-\theta)} - e^{i(\alpha-\theta)}\right](r^2/\varsigma) - iU_v\left[e^{-i(\alpha-\theta)} - e^{i(\alpha-\theta)}\right](r^2/\varsigma) + (i\Gamma/2\pi)\ln\varsigma - i\Omega(r^4/\varsigma^2) \tag{15}$$

The first term in Eq. (15) denotes the complex potential resulting from the uniform translation of the airfoil with speed U_∞ and incidence α, the second term is from the oscillation in the flight direction with velocity $U_h(t)$, the third term is from the vertical plunging motion with velocity $U_v(t)$, and the last term are caused by the circulation and rotation of the airfoil with angular velocity

$$\Omega(t),\ \theta = \int \Omega\,\mathrm{d}t$$

is the angle of rotation.

The complex velocity in the circle plane is

$$Q \equiv \frac{\mathrm{d}W}{\mathrm{d}\varsigma}$$

and in the cylinder (airfoil) plane

$$Q \equiv \frac{\mathrm{d}W}{\mathrm{d}\varsigma} = \frac{\mathrm{d}W}{\mathrm{d}\varsigma}\frac{1}{\mathrm{d}Z/\mathrm{d}\varsigma} = \frac{\mathrm{d}W}{\mathrm{d}\varsigma}\frac{1}{1 - r^2/\varsigma^2}$$

Thus, the complex velocity distribution along the body surface is

$$Q_{\text{abs}} \equiv (U - iV)_{\text{abs}} = [1/(e^{-i2\Psi} - 1)]\Big\{U_\infty\left[e^{-i(\alpha-\theta)} - e^{i(\alpha-\theta)}\right] - U_h\left[e^{-i(\alpha-\theta)} - e^{i(\alpha-\theta)}\right] + iU_v\left[e^{-i(\alpha-\theta)} + e^{i(\alpha-\theta)}\right] - i(\Gamma/2\pi r)e^{-i\Psi} - i2\Omega r e^{i\Psi}\Big\} \tag{16}$$

At the trailing edge $\varsigma = r(\Psi = \pi)$, we employ the Kutta condition. Thus the bracketed term must vanish, and we obtain the value of Γ required to meet the Kutta condition

$$\Gamma = \pi c[U_\infty \sin(\alpha - \theta) - U_h \sin(\alpha - \theta) - U_v \cos(\alpha - \theta) - \Omega c/4] \tag{17}$$

However, the velocity just derived is an absolute velocity of the fluid motion generated by the airfoil movement. The velocity relative

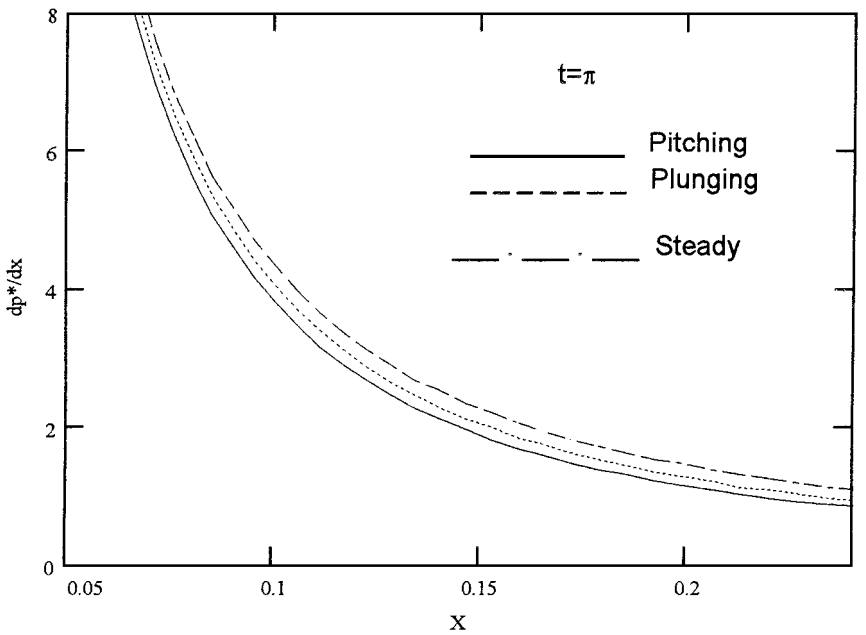

Fig. 3 Comparison of effective pressure gradients.

to the airfoil surface is then obtained by subtracting the rigid-body motion of the airfoil from the absolute velocity.

The complex velocity of the airfoil surface caused by rigid-body motion is given by

$$Q_{\text{ref}} \equiv (U - iV)_{\text{ref}} = -U_\infty e^{-i(\alpha-\theta)} + U_\infty e^{-i(\alpha-\theta)} - iU_\infty e^{-i(\alpha-\theta)} + (i\Omega c/2)\cos\Psi \tag{18}$$

After some algebraic handling, the relative velocity distribution U along the airfoil is found to be

$$U \equiv |Q_{\text{abs}} - Q_{\text{ref}}| = (1/\sin\Psi)[U_\infty \sin(\alpha - \theta + \Psi) - U_h \sin(\alpha - \theta + \Psi) - U_v \cos(\alpha - \theta + \Psi) + \Gamma/\pi c + (\Omega c/4)\cos 2\Psi] \tag{19}$$

When normalised by the uniform velocity U_∞ and the chord c and substituted into the expression for the circulation, Eq. (19) in its nondimensional form reads

$$U = [1/\sin(\Psi/2)][\sin(\alpha - \theta + \Psi/2) - U_h \sin(\alpha - \theta + \Psi/2) - U_v \cos(\alpha - \theta + \Psi/2)] - K\Omega \sin\Psi \tag{20}$$

Equation (20) provides the far-field condition for the boundary-layer formulation described in preceding section.

IV. Pitching and Plunging Oscillations

Now we discuss the problem of the equivalence between fluid motions generated by pitching and plunging airfoils. The inviscid velocity distribution U, in nondimensional form, along the contour of the thin airfoil is given by

$$U_{\text{PL}} = [1/\sin(\Psi/2)][\sin(\alpha + \Psi/2) - U_0 \sin t \cos(\alpha + \pi/2)] \tag{21}$$

for a plunging oscillation with $U_v = U_0 \sin t$, and

$$U_{\text{PT}} = [1/\sin(\Psi/2)]\sin(\alpha - \theta + \Psi/2) - K\theta_0 \cos t \sin\Psi \tag{22}$$

for a pitching oscillation with $\theta = \theta_0 \sin t$, $\Omega = \mathrm{d}\theta/\mathrm{d}t = \theta_0 \cos t$.

Let us compare U_{PL} with U_{PT} using the assumed equivalence relationship $\theta_0 = U_0$. At the leading edge both distribution have a singularity caused by the thin airfoil approximation used. Figure 3 shows at the beginning of the α-increasing phase ($t = \pi$) the distributions of effective pressure gradient over pitching and plunging thin airfoils (approximated to a flat plate), both oscillating with equivalent amplitude $\theta_0 = U_0 = 0.1$ around the same mean angle of attack $\alpha = 10$ deg at the same reduced frequency $K = 1$. A significant difference between the two results is observed near the leading edge. Figure 4 shows the angle of attack for which the effective pressure gradient become equal with steady flow pressure gradient in the vicinity of the leading edge ($x/c = 0.1$) as function of reduced frequency parameter K. These results confirm that the two oscillation modes differ in the sense that the boundary layer separates differently.

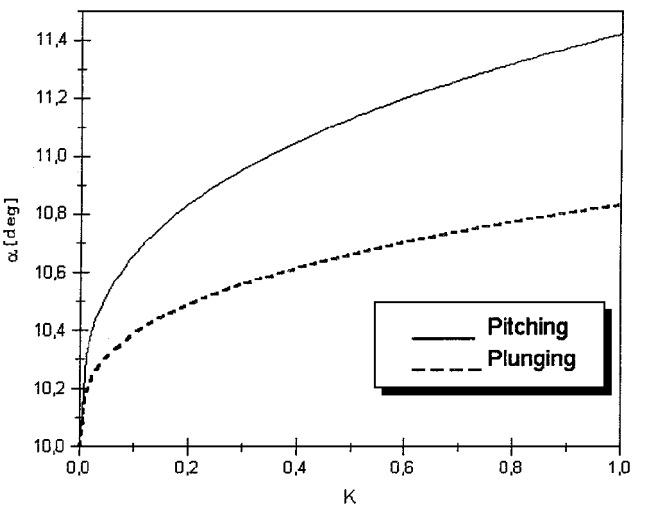

Fig. 4 Incidence for $(\mathrm{d}p/\mathrm{d}x)_{\text{unst}} = (\mathrm{d}p/\mathrm{d}x)_{\text{st}}$ as a function of reduced frequency.

V. Conclusions

The boundary-layer equations have been formulated in a noninertial frame fixed to an arbitrarily moving body. The only additional term in the tangential momentum equations is that caused by the Coriolis force resulting from the body rotation. For two-dimensional flow the boundary-layer approximation have led to the same forms as in usual inertial cases. The development of the boundary layer is determined solely by the effective pressure gradient, defined in terms of relative velocity, which is a measure of the combined effect of both inviscid and viscous forces resulting from the body motion. Thus, the potential flow distribution around an arbitrarily accelerating body has also been derived, and the effective pressure gradient

term has been calculated. A comparison of effective pressure gradients over pitching and plunging thin airfoils has been made. The results show that the similarity between the two oscillatory motions, often assumed in the dynamic stall analyses, is not correct because of different leading-edge separation.

References

[1]Ericsson, L. E., "Moving Wall Effects in Unsteady Flow," *Journal of Aircraft*, Vol. 25, No. 11, 1998, pp. 977–990.

[2]Maresca, C. A., Favier, D. J., and Rebont, M. J., "Unsteady Aerodynamics of an Airfoil at High Angle of Incidence Performing Various Linear Oscillations in a Uniform Stream," *Journal of the American Helicopter Society*, Vol. 3, No. 4, 1981, pp. 40–45.

[3]McCroskey, W. J., "The Phenomenon of Dynamic Stall," NASA TM 81264, March 1981; also Paper 2, von Kármán Inst. Lecture Series, March 1981, pp. 2.1–2.15.

[4]Carta, F. O., "A Comparison of the Pitching and Plunging Response of an Oscillating Airfoil," NASA CR-3172, Oct. 1979, pp. 117–120.

[5]Schlichting, H., *Boundary Layer Theory*, McGraw–Hill, New York, 1968.

Aerodynamic Suppression of Wing Rock Using Fuzzy Logic Control

A. G. Sreenatha*
Australia Defence Force Academy,
Canberra, Australian Capital Territory 2600, Australia
and
N. K. Nair† and K. Sudhakar‡
Indian Institute of Technology,
Powai, Mumbai 400 076, India

I. Introduction

WING rock is a limit-cycle roll oscillation experienced by aircraft with sweptback wings at high angles of attack. The amplitude and frequency of wing rock is a nonlinear function of many parameters such as angle of attack, side slip, etc. Nayfeh et al.[1] have suggested an approximate nonlinear mathematical model to describe the wing rock phenomenon.

Several theories have been put forward over the years to explain the wing rock phenomenon. Some of the factors, which emerge out of these, are as follows. 1) Wing rock is initiated because of vortex asymmetry.[2] 2) Vortex bursting does not initiate wing rock, but plays an active part in limiting the amplitude of the limit cycle.[3] 3) There is negative roll damping at small angles of bank and positive roll damping at higher angles of bank.[4] 4) Wing rock is caused by the relative time lag between the static and dynamic position of vortex normal to the wing surface.[5]

These studies indicate that the vortex formation plays an important role during wing rock. Hence, one can manipulate these vortices suitably for achieving wing rock suppression. Various techniques have been used for aerodynamic suppression of wing rock with this vortex manipulation. Some of them are 1) steady and pulsed blowing,[6] 2) tangential leading-edge blowing,[7] 3) spanwise blowing,[8] and 4) recessed angle spanwise blowing (RASB).[9] In addition to these blowing techniques, efforts have been made to alter the behavior of the vortices using sharp-edged deflectors[10] and apex flaps.[11]

Paralleling these experimental efforts to study and suppress the wing rock phenomenon, various control techniques have been tried employing the approximate mathematical model. Some of the prominent ones are 1) optimal control-based techniques,[12,13] 2) use of fuzzy logic control (FLC) for suppression,[14] and 3) suppression using neural networks.[15,16] These methods have shown to be very successful in suppressing the wing rock numerically.

For most engineering systems, there are two important information sources. The sensors that provide numerical measurement of the variable of interest are the first source and another is the human expert who provides linguistic information about the system. Conventional engineering approaches have difficulty in incorporating this linguistic information. This results in a lot of valuable information being lost. A knowledge-based system[17] can be defined as a system in which the performance, reliability, and robustness of the system is improved by incorporating knowledge that cannot be accommodated in the analytical model and that is normally taken care of by the manual modes of the operator or by other safety and ancillary logic mechanisms. FLC[18] belongs to this class of knowledge-based systems, places more emphasis on the linguistic information, and is primarily concerned with the input output behavior of the plant. Hence, FLCs are robust and can be used to control processes whose mathematical models are not well defined or are nonlinear. The present work aims at suppressing the wing rock by the RASB technique. To control the amount of blowing and the direction of blowing, a simple FLC is derived. The FLC is developed without assuming a mathematical model of the system. For constructing the rule base, experience is gained by carrying out some initial experiments in the wind tunnel. A brief description of the FLC is provided in Sec. II. The development of the FLC based on the experimentation is outlined in Sec. III. Section IV discusses the experimental results with the FLC. The paper is concluded in Sec. V, outlining some future work.

II. FLC[17]

The FLC is based on the fuzzy set and fuzzy logic that is closer in spirit to human thinking and natural language than traditional logic systems. Figure 1 shows the block diagram of an FLC. The FLC consists of fuzzification, decision making, knowledge base, and defuzzification blocks. For the sake of completeness, the various blocks are discussed very briefly in the following paragraphs.

Fuzzification maps the crisp input variables into fuzzy variables with their associated degrees of membership. Thus, each value of the input variable is transformed into fuzzy term sets with associated degrees of memberships. Once the degrees of memberships of the crisp inputs are known, they are passed onto the decision making logic (DML) block. DML refers to the knowledge base for processing the data.

The knowledge base primarily consists of a rule base and a database. The rule base consists of fuzzy IF–THEN statements; the IF part is the rule antecedent, and the THEN part is the rule consequent. The rule base is used to represent in a structured way the control policy of an experienced process operator and/or the control engineer. The rule base characterizes the control goals and the control policies of the domain experts by means of linguistic rules such as the following: If error e is negative big (NB) then control input u is positive big (PB). The defuzzification block is used to convert fuzzy outputs of the DML to crisp outputs to be given to the real world. This is the inverse of fuzzification.

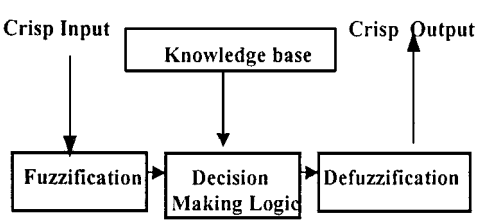

Fig. 1 Block diagram of FLC.

Received 4 August 1999; accepted for publication 31 August 1999.

*Lecturer, School of Aerospace and Mechanical Engineering, University College.
†Master of Technology Scholar, Department of Aerospace Engineering.
‡Professor, Department of Aerospace Engineering.